International Journal of Heat and Fluid Flow 30 (2009) 218–228

Contents lists available at ScienceDirect

International Journal of Heat and Fluid Flow

journal homepage: www.elsevier.com/locate/ijhff

Numerical analysis of turbulent convection heat transfer from an array of perforated fins ☆

M.R. Shaeri, M. Yaghoubi *

Mechanical Engineering Department, School of Engineering, Shiraz University, Shiraz 71348-51154, Iran

ARTICLE INFO

Article history:
Received 21 May 2008
Received in revised form 23 December 2008
Accepted 29 December 2008
Available online 15 February 2009

Keywords:
Heat transfer enhancement
RNG model
Perforated fins
Fin optimization
Fin effectiveness
Turbulent flow

ABSTRACT

Numerical investigation is made for three-dimensional fluid flow and convective heat transfer from an array of solid and perforated fins that are mounted on a flat plate. Incompressible air as working fluid is modeled using Navier–Stokes equations and RNG based $k-\varepsilon$ turbulent model is used to predict turbulent flow parameters. Temperature field inside the fins is obtained by solving Fourier's conduction equation. The conjugate differential equations for both solid and gas phase are solved simultaneously by finite volume procedure using SIMPLE algorithm. Perforations such as small channels with square cross section are arranged streamwise along the fin's length and their numbers varied from 1 to 3. Flow and heat transfer characteristics are presented for Reynolds numbers from 2×10^4 to 4×10^4 based on the fin length and Prandtl number is taken $Pr = 0.71$. Numerical computations are validated with experimental studies of the previous investigators and good agreements were observed. Results show that fins with longitudinal pores, have remarkable heat transfer enhancement in addition to the considerable reduction in weight by comparison with solid fins.

1. Introduction

Rapid heat removal from heated surfaces and reducing material weight and cost has become a major task for design of heat exchanger equipments. Development of super heat exchangers requires fabrication of efficient techniques to exchange great amount of heat between surfaces such as extended surfaces and ambient fluid. Bluff plates as extended surfaces or fins are good heat transfer equipments that are widely used for various industrial applications. Fluid flow and heat transfer over rectangular bluff plates has been the main subject of many researches. Studies about three dimensional bluff plates are extensive. Asako and Faghri (1994) studied numerically periodic fully developed fluid flow and heat transfer characteristics of turbulent flow over three-dimensional arrays of heated square blocks deployed along one wall of a parallel-plate duct that refers to forced convection cooling of electronic equipments. They applied high Reynolds number form of the $k-\varepsilon$ turbulence model for their analysis. Computations are performed for condition of uniform wall temperature, for a wide range of geometric parameters and Reynolds numbers from 10^4 to 10^5. Meinders et al. (1998) performed experiments for a single array of wall mounted cubical protrusions along a channel to measure local convective heat transfer using infrared and liquid crystal thermography as well as oil-film visualization. They indicated that for low Reynolds numbers range 795–6656, fluid flow and heat transfer highly depends on block position in the row. Nakamura et al. (2001) extended experimental investigation for fluid flow and heat transfer around a cube mounted on a wall of a plane in a turbulent boundary layer for Reynolds numbers of the range 4.2×10^3–3.3×10^4. Niceno et al. (2002) studied turbulent flow and heat transfer for a matrix of blocks. They presented a new review for various measurements and different RANS modeling simulation and applied large eddy simulation to study fluid flow and heat transfer from an internally heated multi-layered matrix of cubes mounted on a surface of a channel. They have found vortex structure and their relation with heat transfer and temperatures distribution.

Three-dimensional studies of convective heat transfer around an array of non-cubical rectangular bluff plates are scarce. El-Sayed et al. (2004) investigated experimentally turbulent heat transfer, fluid flow and pressure drop characteristics of longitudinal rectangular-fin array for three different orientations of tested models: (1) parallel flow, (2) impinging flow, and (3) reverse impinging flow, to determine the optimal position of fin array in the flow field. They reported that the parallel flow case yielded highest heat transfer rate and lowest pressure drop followed by the impinging flow than the reverse impinging flow cases. Also Velayati and Yaghoubi (2005) numerically studied turbulent fluid flow and heat transfer characteristics of heated rectangular plates mounted over a surface. Their investigation included effects of variation of the plate blockage ratio and flow Reynolds number. Jonsson and Moshfegh (2001) performed experiments in a wind tunnel with seven types

☆ Academy of Sciences I. R. Iran.

* Corresponding author. Tel./fax: +98 711 2303051.
E-mail address: yaghoub@shirazu.ac.ir (M. Yaghoubi).

0142-727X/$ - see front matter © 2009 Elsevier Inc. All rights reserved.
doi:10.1016/j.ijheatfluidflow.2008.12.011

Nomenclature

A	area
A_D	reference area applied in drag coefficient
A_F	frontal area of fin
A_T	total fin area including outer surface and inner surface of perforation
A_V	area applied in friction drag
ΔA	computational cell area
$\overline{C_D}$	average total drag coefficient
C_f	local skin friction coefficient
D, H, L, S	fin thickness, height, length, spacing
F_F, F_P, F_D	friction, form, total drag force
Gr	Grashof number
$h, \overline{h}$	local and average convection heat transfer coefficient
H_P, W_P	perforation height and width
k	turbulent kinetic energy
N	number of perforations
n	normal direction to the surface of fin and perforation
$\overline{Nu}$	average Nusselt number, $\frac{\overline{h}L}{\lambda}$
Pr	Prandtl number
q	heat transfer rate from fin surface
Q	total heat dissipation rate from heat sink
Re	Reynolds number
Re_L	Reynolds number, $(u_\infty L)/\nu$
R_{th}	thermal resistance of heat sink
T	temperature
U	total fluid velocity
u, v, w	velocity components in X,Y,Z directions
V, V_{void}	fin volume $(L \times H \times D)$ and void volume $(L \times H_P \times W_P \times N)$
X, Y, Z	cartezian coordinates

Greek symbols

ε	turbulent dissipation rate
ε_f	fin effectiveness
ϕ	porosity, $(\frac{V_{void}}{V})$
λ	fluid thermal conductivity
ν	fluid kinematics viscosity
ρ	fluid density
$\tau_w, \overline{\tau_w}$	local and average wall shear stress

Subscripts

b	fin base
DS, US	downstream and upstream
Dh	hydraulic diameter
hs	heat sink
i	summation index
in	inside of perforation
S	fin surface
∞	free stream

of heat sinks including plate fin, strip fin, and pin fin heat sinks. They developed an empirical bypass correlation for different fin designs. Their correlation predicts Nusselt number and dimensionless pressure drop. Yu et al. (2005) performed experimental and numerical studies to compare thermal performances of plate fin heat sinks and plate-pin fin heat sinks. They reported that resistance of a plate-pin fin heat sink was about 30% lower than that of a plate fin heat sink used to construct the plate-pin fin heat sink under the condition of equal fluid air velocity. Yakut et al. (2006) experimentally analyzed the effects of heights and widths of hexagonal fins, streamwise and spanwise distances between fins and flow velocity on their thermal resistance and pressure drop characteristics. Li and Chen (2007) used infrared thermography technique to investigate thermal performance of plate-fin heat sinks under confined impinging jet conditions and discussed the influence of Reynolds number and geometry.

Heat transfer rate from fins can be improved by employing perforations, porosity or slots (Sahin and Demir, 2008). On the other hand, because of limitation in space and economical reasons, heat transfer equipments have been required to be much more compact in size and light in weight (Fujii et al., 1988). So while a simple solid baffle plate attached to the duct wall enhances heat transfer, a perforated plate attached to the same duct wall poses less resistance to the flow and, thus, might have a better performance (Molki and Hashemi-Esfahanian, 1992). So far by use of perforated fins, one can gain both goals of fin optimization. The research of flow visualization and heat transfer for perforated plates and fins has been addressed in many studies. Sparrow and Carranco Ortiz (1982) experimentally determined heat transfer coefficient on an upstream facing surface that was contained a regular array of holes that were arranged on equilateral triangular centers. In their experiments, two parameters as hole pitch to diameter ratio and Reynolds number for each hole were varied. Fujii et al. (1988) studied fluid flow and heat transfer experimentally from a type of heat exchanger that consist of a surface which was bent to form a trapezoidal shape and had many perforations. They obtained dimensionless correlations for Nusselt number and drag coefficient in manner of optimum design of compact heat exchangers. Sara et al. (2000) determined thermal performances of solid and perforated rectangular blocks that are attached on a flat surface in a rectangular duct in comparison with heat transfer from the same plate without blocks. They reported that the solid blocks generated a net energy loss despite significantly enhanced heat transfer due to the increased heat transfer surface area. Also they founded that the increase of Reynolds number conducted to decrease in the performance of both solid and perforated blocks. Sahin and Demir (2008) experimentally investigated variation of overall heat transfer, friction factor and effect of various design parameters on heat transfer and friction factor for heat exchangers equipped with square cross sectional perforated pin fins in a rectangular channel. They considered effects of flow and geometrical parameters on heat transfer and friction characteristics and also obtained correlations for the efficiency enhancement. Configuration of perforated fins in the study of Sahin and Demir (2008) is similar to the present study but in the present study only an array of perforated fins in one row is considered, in addition the shape of perforations are rectangles. Dorignac et al. (2005) experimentally determined convective heat transfer on a multi perforated plates. For a large range of perforations spacings, they proposed an empirical relation for heat exchange at windward surface of a perforated flat plate. They reported that convective exchange on the upstream side of a multi perforated plate depends on the pitch between perforations. Also they reported that to calculate the mean convective exchanges around perforations, one must define Nusselt and Reynolds numbers on characteristics (length and velocity) linked to the upstream side and not to the perforations. Other studies about perforated plates can be found in Nilles et al. (1995), Souidi and Bontemps (2001), Hwang and Liou (1995), Hwang et al. (1998), Liou and Chen (1998) and Torii and Yang (2002).

The aim of the present study is to determine thermal performance of a new type of perforated fins and comparing their results with solid fin and the flat surface without fins for the same

conditions. For this consideration, three-dimensional turbulent fluid flow and convective heat transfer around an array of solid and perforated rectangular fins are analyzed numerically. Fins have perforations with square cross section and assumed to be 1, 2 and 3. These perforations are along the fin and their cross section is perpendicular to the fluid flow direction. Selecting smaller size makes the flow laminar in the channel and increasing more channels is not possible due to fin dimension and shape. As far as the authors are aware, detailed experimental or theoretical work on flow and heat transfer for an array of three-dimensional perforated fins with the shape presented in this study mounted on a flat plate with the selected perforation seems to be limited and the present analysis maybe the first study with turbulent flow regime.

2. Problem description and boundary conditions

Typical presentations of bluff plates modeled in this study are shown in Fig. 1. The airflow is considered to be steady and turbulent with constant properties. Moreover, air velocities are such that forced convection is the dominant heat transfer mechanism between fins and ambient air and in the perforations. The corresponding Richardson number $\left(\frac{Gr}{Re^2}\right)$ based on the fin height is less than 0.001, therefore the effect of free convection is negligible. Fin material is assumed to be aluminum with thermal conductivity 202 W m^{-1} K^{-1}. Such fins are widely used for heat removal from heating surfaces. Fins have the length, height and thickness equal to 24, 12 and 4 mm, respectively, and the fin spacing is assumed to be 10 mm. Each perforation has height and width equal to 3 mm and their length is equal to the fin's length. The fin's length is used as the characteristic length in the Reynolds number. Studies are made for Reynolds number $Re_L = \frac{u_\infty L}{\nu}$ in the range of 2×10^4–4×10^4. This range of Reynolds number covers velocities around 13.07 m/s–26.14 m/s. These velocities are chosen such that the flow inside the perforations be also turbulent and flow field be applicable for cooling from heat removal elements. Corresponding Reynolds number inside the perforations is 2500–5000 based on the hydraulic diameter of the perforations (ducts). It should be noted that for solid fin and fin with 1 perforation the flow at high Reynolds numbers becomes unsteady whereas by increasing

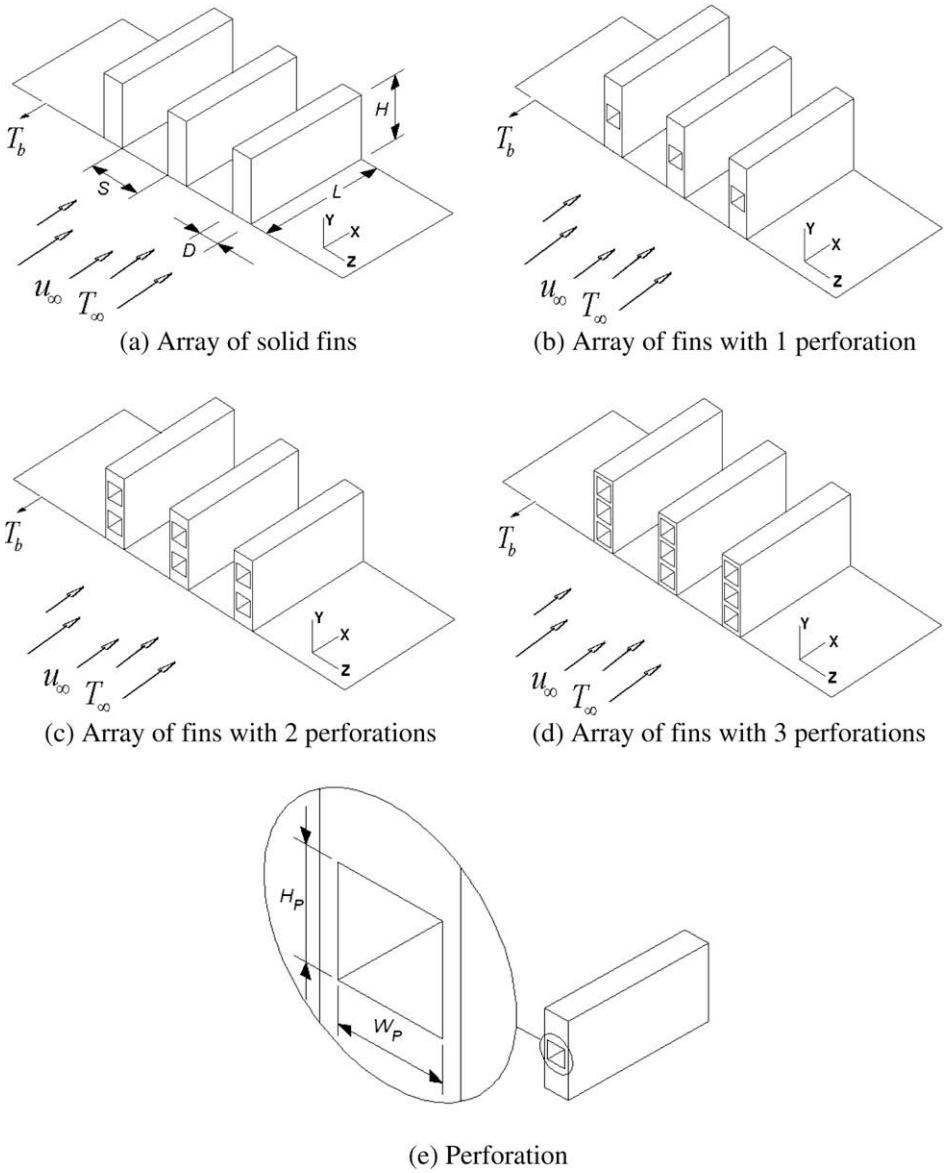

(a) Array of solid fins

(b) Array of fins with 1 perforation

(c) Array of fins with 2 perforations

(d) Array of fins with 3 perforations

(e) Perforation

Fig. 1. Various fin arrays of solid and perforated configuration.

Table 1
The range of Reynolds number studied for steady state flow.

Fin type	Re_L	Re_{Dh} in duct
Solid fin	2×10^4–2.5×10^4	2500–3126
Fin with 1 perforation	2×10^4–3×10^4	2500–3749
Fin with 2 perforations	2×10^4–4×10^4	2500–5000
Fin with 3 perforations	2×10^4–4×10^4	2500–5000

number of perforations the flow remains steady at such Reynolds numbers. Table 1 shows the range of Reynolds number studied where the flow remained steady and computations converged to appropriate results.

Due to uniform air flow parallel to the fins and symmetry, computations are applied only for one fin instead of array of fins. Fig. 2 shows the computational domain. Domain used in this study is similar to the domain used in (Velayati and Yaghoubi 2005) with differences that Velayati and Yaghoubi (2005) considered one half of fin but in the present study the whole fin is considered to capture any possibility of non-symmetry. For the plane *abcd*, as inlet boundary, uniform flow condition is considered for all variables using $u_{in} = u_\infty$, $v_{in} = w_{in} = 0$ and $T_{in} = T_\infty$. Also the same conditions are applied for plane *bckj* that is free stream plane. For plane *ijkl* that is outlet and far from the plate, zero gradients of variables in the X direction, $\frac{\partial()}{\partial X} = 0$ are imposed. This condition is for fully developed condition but it can be applied at this simulation because the outlet boundary is sufficiently far from the plate. For planes *abji* and *dckl*, symmetry conditions are applied that means zero gradients of variables in the Z direction, $\frac{\partial()}{\partial Z} = 0.0$, and also in these planes $w = 0$. All remaining planes are solid walls with no slip boundary condition. Free stream temperature is assumed 25 °C and the fin base, plane *efgh*, assumed to have a constant temperature equal to 70 °C. Also the planes *adeh* and *fgil* are assumed adiabatic. It has been reported that thermal radiation rate is less than 5% and 8% of total heat transfer rate from the finned surfaces for polished aluminum fins for temperature differences around 40 °C and 77.5 °C (Leung and Probert 1989). For the present computation, the effect of radiation heat transfer is neglected, since the maximum temperature difference is 45 °C.

3. Governing equations

Governing equations for the three-dimensional steady state incompressible fluid flow and turbulent modeling RNG $k-\varepsilon$ are the same as used by Velayati and Yaghoubi (2005). For calculation of temperature field in the fin's surfaces and perforation's walls, conjugate problem of Fourier's steady state heat conduction equation with convection in the fluid are solved simultaneously.

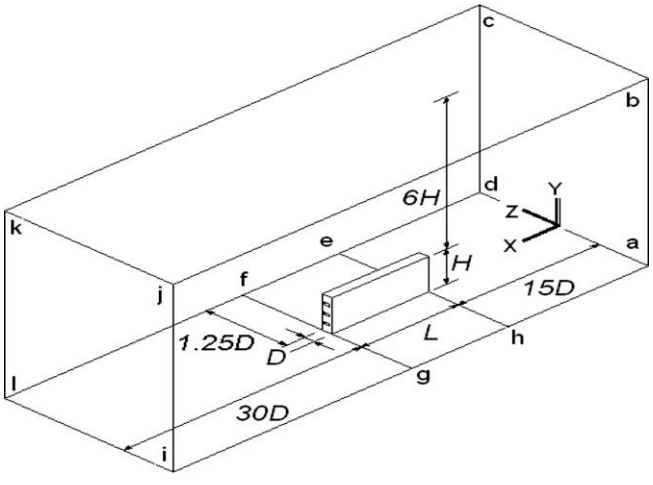

Fig. 2. Computational domain for solid and perforated fins.

4. Computational scheme

4.1. Domain geometry and grid size

The domain used in the present study is illustrated in Fig. 2. It consists of an entrance region, an exit plane and the upper free stream surface that are planes *abcd*, *ijkl* and *bckj*, respectively. These planes should be sufficiently far from the fin surfaces that the results become independent of the boundary positions. For this reason some tests were performed for obtaining an appropriate distance from the fin surfaces that can be found in Velayati and Yaghoubi (2005) and Yaghoubi et al. (2002). In the present study, after several tests and using numerical experience of the previous studies, the computational domain is chosen 15D upstream, 30D downstream, 7H in Y direction and 3.5D in Z direction. The next stage is generation of appropriate grid points in the three dimensions. For proper capture of recirculation zone and reattachment point, the grid arrangement must be dense near the fin surfaces and perforation walls. The grid configuration for solid and perforated fin with 1 perforation is shown in Fig. 3. The solution must be independent of grids, and to reach independency, several grid configurations were studied. The grid study was performed by changing the number of grids in three dimensions and for each grid average wall shear stress and average Nusselt number is determined. The related calculations as a sample for fin with 1 perforation are reported in Table 2.

Table 2 shows that the number of grid points in the X, Y and Z directions of $200\times101\times61$ for fin with 1 perforation are appropriate. For to more dense grids, the changes of related parameters are less than 1%. For this geometry the grid resolution in the perforations is 0.2 mm or less than 6.7% of the channel width. For solid and other perforated fins the same procedure is repeated.

4.2. Computational procedure

The governing equations are discretized using a finite volume code. In the discretization scheme, control volume cells for velocity components are staggered with respect to the main control volume cells using the SIMPLE algorithm developed by Patankar (1980). The QUICK technique is used to calculate velocity components, k, ε and energy equations. The set of discretized equations are solved iteratively line-by-line. Computation is started by first solving continuity, momentum, k and ε equations to determine the flow field and then the energy equation to find the thermal field in the computational domain.

4.3. Validation

For the model of perforated fins of the present study there is not any related experimental or numerical investigation. To validate the computations, numerical results for three dimensional solid fins are compared with the experimental measurements of Jonsson and Moshfegh (2001). They performed several experiments for different heat sinks that one of their tested heat sinks as plate fin heat sink is similar to the array of solid fins in the present study. In their experiment as shown in Fig. 4, plate fins had length, height and thickness equal to 52.8, 10 and 1.5 mm, respectively, and spaces between fins were 5 mm. Also wind tunnel had width and height of 63 and 10 mm, respectively. The base of the heat sink was heated uniformly with 10 W. For validation, the array of solid fins like the heat sink in the experiment of Jonsson and Moshfegh (2001) is modeled for the same fluid and thermal conditions, and

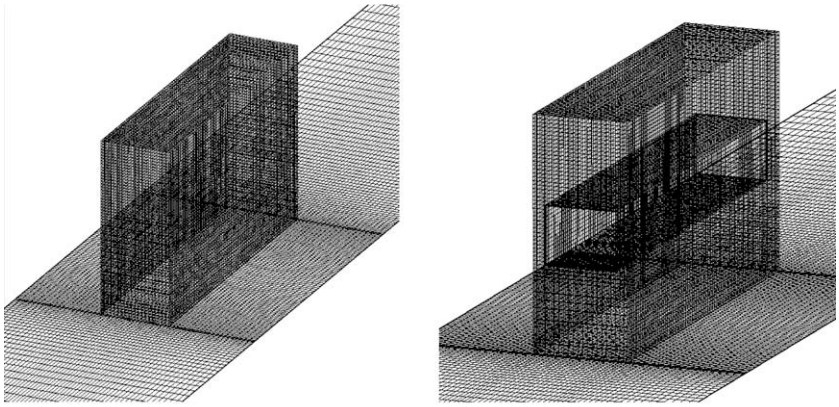

(a) Solid fin (b) Perforated fin with 1 perforation

Fig. 3. Typical grid configurations for solid and perforated fins.

Table 2
Grid independent studies for fin with 1 perforation ($Re_L = 2 \times 10^4$).

Grid in whole domain	Grid in perforation	$\overline{Nu}$	$\overline{Nu}_{in}$	$\overline{\tau_w}$	$\overline{\tau_w}_{in}$
$130 \times 46 \times 22$	$50 \times 4 \times 4$	108.22	94.05	0.78580	1.0000
$155 \times 62 \times 32$	$60 \times 8 \times 8$	110.64	109.53	0.80511	1.2214
$175 \times 75 \times 48$	$70 \times 10 \times 10$	120.96	109.79	0.91292	1.2570
$200 \times 101 \times 61$	$80 \times 15 \times 15$	125.11	109.84	0.97344	1.2961
$225 \times 119 \times 68$	$90 \times 18 \times 18$	125.65	109.92	0.97755	1.3087
$250 \times 130 \times 76$	$100 \times 20 \times 20$	125.82	110.01	0.97923	1.3129

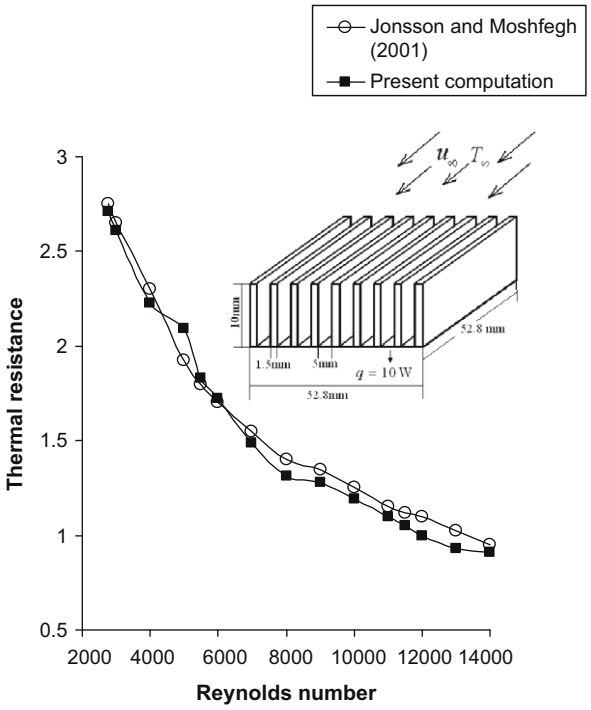

Fig. 4. Comparison of numerical and experimental results for a solid fin with constant heat flux.

results are compared. In the experiment, thermal resistance of heat sinks is calculated by:

$$R_{th} = \frac{1}{\overline{h} A_{hs}} \tag{1}$$

where A_{hs} is the total heat transfer area of heat sink. In addition they calculated the average heat transfer coefficient as:

$$\overline{h} = \frac{Q}{A_{hs}(T_b - T_\infty)} \tag{2}$$

where Q is the total heat dissipation from the heat sink. Temperature in the inlet of wind tunnel was held at approximately 20 °C. Comparison between present numerical results and experimental measurements is illustrated in Fig. 4.

In Fig. 4, Reynolds number is based on the hydraulic diameter of wind tunnel according to definition of Jonsson and Moshfegh (2001). This figure shows a good agreement between the present numerical results and experimental measurements. Therefore with valid numerical modeling, computations will be conducted for new perforated fins.

5. Results and discussion

Analysis of flow field and convection heat transfer for conjugate problem is carried out for $Re_L = 2 \times 10^4 - 4 \times 10^4$, $Pr = 0.71$ and array of fins presented in Fig. 1. For each configuration, thermal field in the solid domain is determined by solving conduction equation. Flow path lines around solid and perforated fins at different heights for Reynolds number of 2.5×10^4 are shown in Figs. 5–8. Fig. 5 shows that recirculation length becomes smaller from top surface of the fin to the base plate due to viscous effect of the base plate. The wake behind the solid fin is visible whereas in the case of perforated fin very small wake is composed attached to the base plate and the flow in the channels of perforation eliminates wake formation. In fact for the reason of perforation, a part of flow goes in the perforations like flow in a duct and for fins with more perforations this part increases. For this reason the formed wakes are negligible for fins with perforations but in the case of solid fin, fluid interacts to the front surface of fin and separation occurs. In addition, for perforated fins with lower amount of perforations the fraction of fluid that can enter the perforations reduces and finally the formed wake becomes larger. Figs. 6–8 show these flow structures for various perforated fins.

With perforations, air flows inside the channels. The drag force that acts on the faces of perforated fins differs with that of acting on the surfaces of solid fin. The drag force has two components, one is related to surface shear stress as the friction drag and another is due to a pressure differential in the flow direction resulting from wake formation as form or pressure drag. Friction force, form drag, total drag force and the average drag coefficient are calculated from Eqs. (3)–(6).

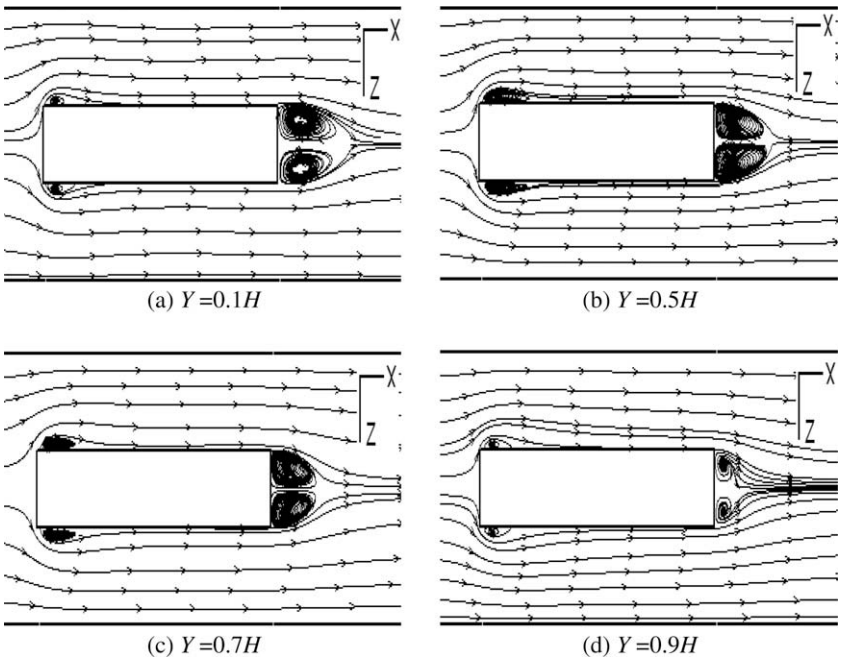

Fig. 5. Flow path lines around solid fin at different heights ($Re_L = 2.5 \times 10^4$).

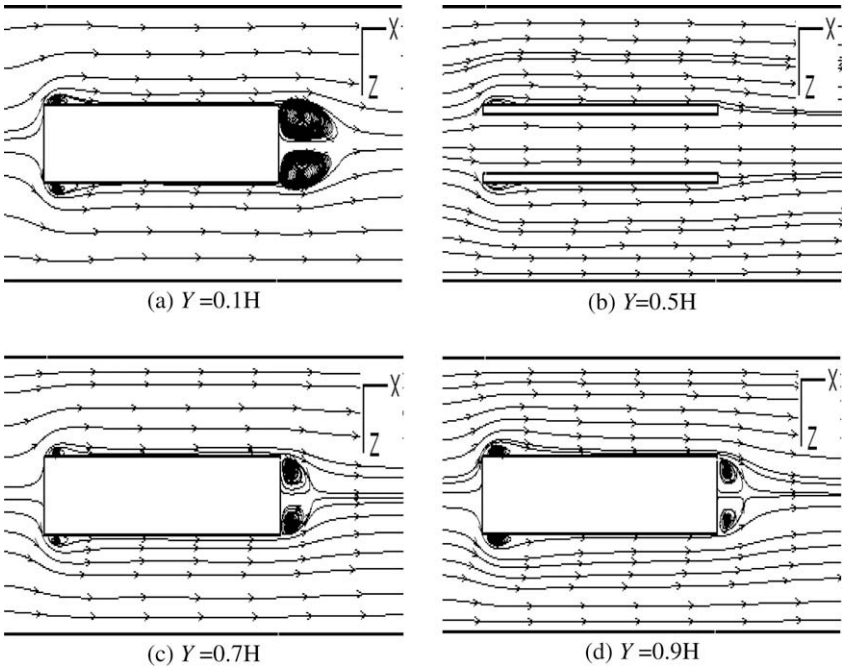

Fig. 6. Flow path lines around perforated fin with 1 perforation at different heights ($Re_L = 2.5 \times 10^4$).

$$F_F = \sum(\tau_w)_i \Delta A_i = \sum \mu \left(\frac{\partial u}{\partial n_i}\right)_S \Delta A_i \tag{3}$$

$$F_P = \left(-\sum P_i \Delta A_i\right)_{US} - \left(-\sum P_i \Delta A_i\right)_{DS} \tag{4}$$

$$F_D = F_F + F_P \tag{5}$$

$$\overline{C_D} = \frac{F_D}{\frac{1}{2} A_D \rho u_\infty^2} \tag{6}$$

In Eq. (3) τ_w is the wall shear stress over the faces of fins, including outer walls of fins and inner walls of perforations. The main consideration in the Eq. (3) is that the area that appears differs for different types of fins. In fact this area is the all surfaces of fin in flow direction that contacts with fluid including outer surfaces of fin and also inner surfaces of perforations. Certainly this area is higher for perforated fins and becomes larger with increase of perforations. The whole surface area of fin that touches fluid in flow direction is given by:

$$A_V = 2H \times L + D \times L + 2N \times L \times H_P + 2N \times L \times W_P \tag{7}$$

In Eq. (4) ΔA_i refers to each computational cell in front and back of the solid part of fin that is perpendicular to the flow stream. For perforated fins the frontal area is much smaller than solid fin and

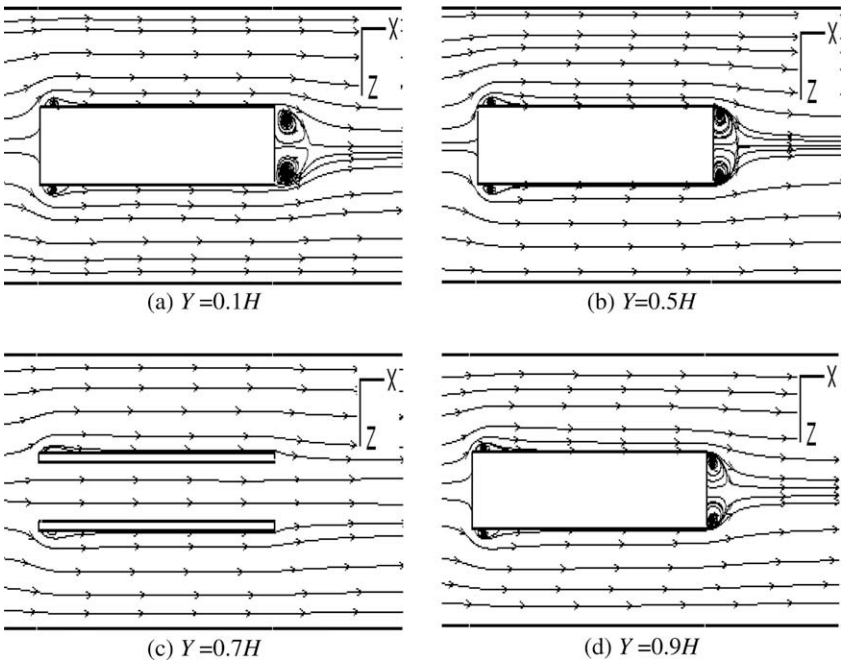

Fig. 7. Flow path lines around perforated fin with 2 perforations at different heights ($Re_L = 2.5 \times 10^4$).

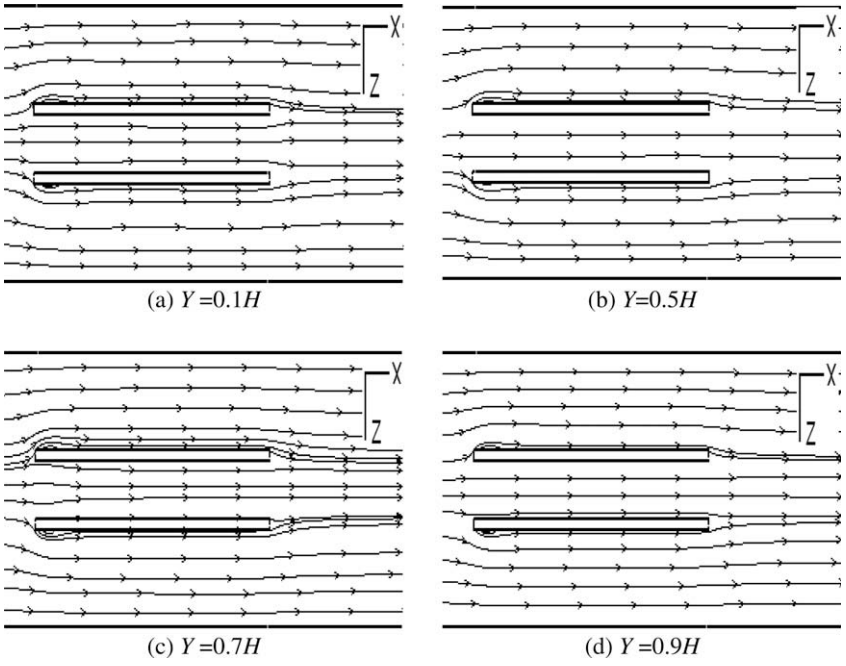

Fig. 8. Flow path lines around perforated fin with 3 perforations at different heights($Re_L = 2.5 \times 10^4$).

becomes smaller by increasing number of perforations. The frontal area for all types of fins is given by:

$$A_F = D \times H - N \times H_P \times W_P \tag{8}$$

It should be noted that in Eq. (6) for accurate comparison of $\overline{C_D}$ for all types of fins, the area 'A_D' is selected the same and equals to the sum of the areas of lateral surface and top surface of fin and it is given by:

$$A_D = 2L \times H + L \times D \tag{9}$$

Figs. 9a–d show variation of friction, form and total drag force in the flow direction and also the average drag coefficient in the flow direction, respectively, for various types of fins. Based on Fig. 9a perforated fins have higher value of the friction drag with respect to solid fin and also friction drag increases with adding number of perforations. The increase in F_F is due to increase in the fin contact area with the fluid in the case of the perforated fins. In fact for perforated fins larger area will touch the fluid, so viscous drag force is larger and it becomes larger with increase of perforations. According to the Fig. 9b solid fin has the largest form drag and its value decreases with increase of perforations. It is mentioned that the wake formed behind the perforated fins are smaller compared to solid fins. For this reason the form drag that results from wake formation decreases with increase in the number of perforations. Fig. 9c shows

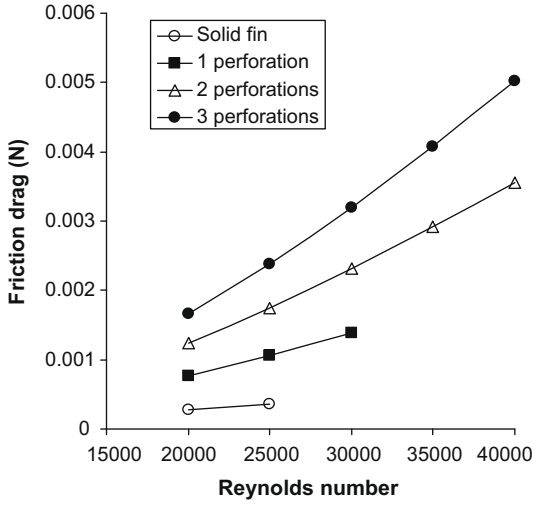

Fig. 9a. Variation of friction drag in flow direction for various types of fins.

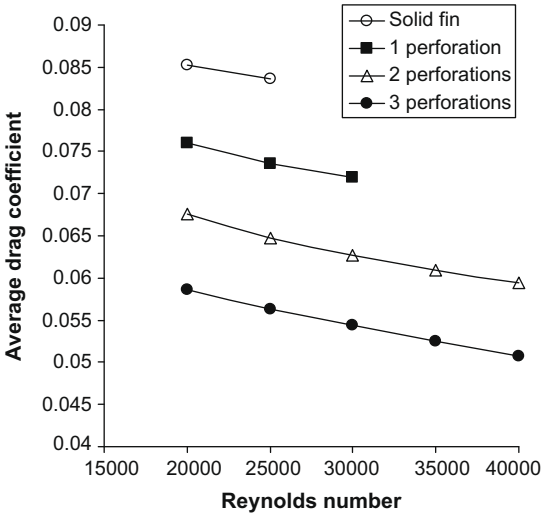

Fig. 9d. Variation of average drag coefficient in flow direction for various types of fins.

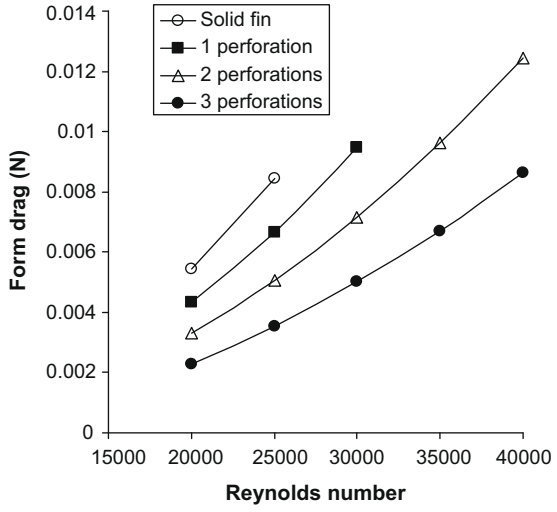

Fig. 9b. Variation of form drag in flow direction for various types of fins.

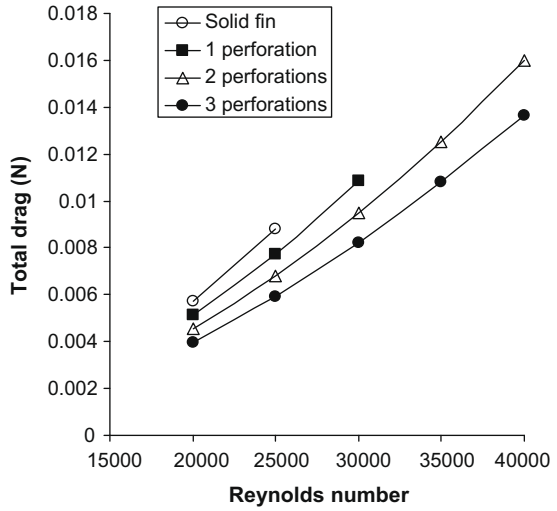

Fig. 9c. Variation of total drag in flow direction for various types of fins.

total drag force according to Eq. (5). Based on Fig. 9c the sum of the friction and form drag shows that total drag force for solid fin is the largest and its value becomes smaller with increase in the number of perforations. In fact the effect of form drag is dominant with respect to viscous drag. Based on Eq. (6) average drag coefficient for various types of fins is illustrated in Fig. 9d. The average drag coefficient has the highest value for solid fin and its value decreases with increase of perforations.

Fig. 10 shows contours of skin friction coefficient over the outer side of solid and perforated fins. Based on Eq. (3), the regions of minimum skin friction coefficient corresponds to the place where wall shear stress is small and these places characterize the reattachment zone. Position of reattachment on the faces of fin is important because maximum value of heat transfer occurs around this region. For three-dimensional blocks, the position of reattachment is an area over fin side face and local skin friction coefficient is calculated from following relation:

$$C_f = \frac{\tau_w}{\frac{1}{2}\rho u_\infty^2} = \frac{\mu\left(\frac{\partial U}{\partial n}\right)}{\frac{1}{2}\rho u_\infty^2} \tag{10}$$

According to Fig. 10, with increase of perforations the length of reattachment zone reduced. Such behavior is illustrated by flow path lines in Figs. 5–8.

Fig. 11 shows temperature distribution over the outer side and top surface of solid fin and fins with various channel holes. Maximum temperature is at the fin base and it reduces to fin tip. Remarkable point in these figures is the increase of temperature drop between the fin base and fin tip by increasing amount of perforations. This confirms the enhancement of heat transfer with increasing number of perforations. Higher temperature difference along the fin height means more heat exchange with air. This is mainly due to more heat transfer area of perforated fins than solid fins. This effect may also be implemented by increasing number of solid fins (making them thinner). The alternate case needs more studies regarding their flow structure, weight reduction, heat transfer coefficient and pressure drop.

Having local temperature over the entire surfaces of the fin, local convection heat transfer is determined by:

$$h = \frac{-\lambda(\partial T/\partial n)_S}{T_S - T_\infty} \tag{11}$$

Average convection heat transfer coefficient and average Nusselt number can be calculated by:

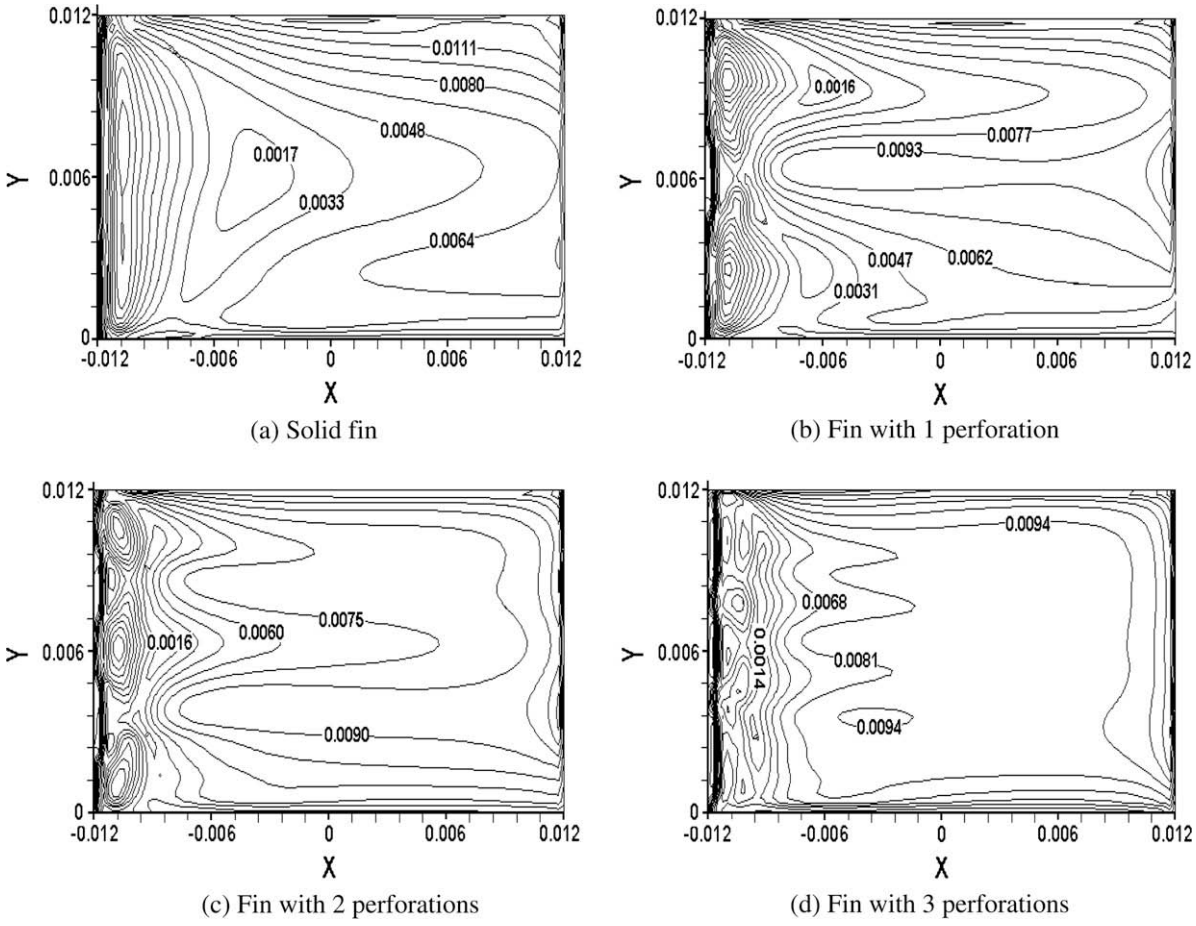

Fig. 10. Contours of skin friction coefficient over the outer surface of various types of fins at ($Re_L = 2.5 \times 10^4$).

$$\overline{h} = \frac{1}{A_T}\sum h_i \Delta A_i \tag{12}$$

$$\overline{Nu} = \frac{\overline{h}L}{\lambda} \tag{13}$$

The area, A_T, in Eq. (12) is the total area of fin that touches fluid, including outer surfaces of fin and inner surfaces of perforations which can be determined by:

$$A_T = 2D \times H + 2H \times L + D \times L - 2N \times H_P \times W_P + 2N \times L \times H_P + 2N \times L \times W_P \tag{14}$$

Variation of average Nusselt number over the faces of solid fin as well as outer and inner surfaces of various perforated fins is illustrated in Fig. 12. It is observable that solid fin has the largest average Nusselt number in comparison with perforated fins. With perforations (channels), some of flow passes along the channels and air velocity reduces and also Nusselt number decreases. Such behavior corresponds to the decrease of total drag with increase of perforations. From this figure average Nusselt number is highest for solid fin and its value decreased with increasing perforations.

To determine fin performance, a parameter such as fin effectiveness (Incropera and DeWitt, 1996) is defined. Fin effectiveness is the ratio of heat transfer from fin to heat transfer from fin base without fin as:

$$\varepsilon_f = \frac{q}{\overline{h_b} A_b (T_b - T_\infty)} \tag{15}$$

In Eq. (15) heat transfer rate is determined by:

$$q = \sum h_i \Delta A_i (T_S - T_\infty) \tag{16}$$

Fig. 13 shows variation of fin effectiveness with Reynolds number. According to Fig. 13 perforated fins have higher effectiveness with respect to solid fin. Fin effectiveness becomes larger with more perforations in such a manner that the difference in fin effectiveness between solid fin and fin with 3 perforations is remarkable and it is higher than 65%.

From Fig. 13, one can find that perforated fins have much higher heat transfer performance and can exchange more heat between primary surface and the ambient air. Even though the average Nusselt number for solid fin is the highest among other types of fins and its value decreases with increase the number of perforations, but perforated fins have larger heat transfer area compared with solid fin and by increase of perforations, heat transfer area becomes larger. This area difference is presented in Table 3. On the basis of Table 3, it is clear that perforated fins make very larger heat transfer area with respect to solid fin and by increasing number of perforations the amount of heat transfer rate will raise. Such design implementation is along fin optimization for industrial applications. Generally optimization of fins is focused on two objects, first to maximize heat dissipation for a given mass or volume and the other is to minimize the mass or volume of fin for a given heat dissipation rate (Razelos and Kakatsios, 2000). Other major advantage of utilizing new perforated fins is their lighter weight in comparison with solid fins. Table 4 shows comparison of weight reduction with respect to solid fin.

It is apparent that with increase of perforations, the fins become lighter, results saving in manufacturing of fins and huge reduction

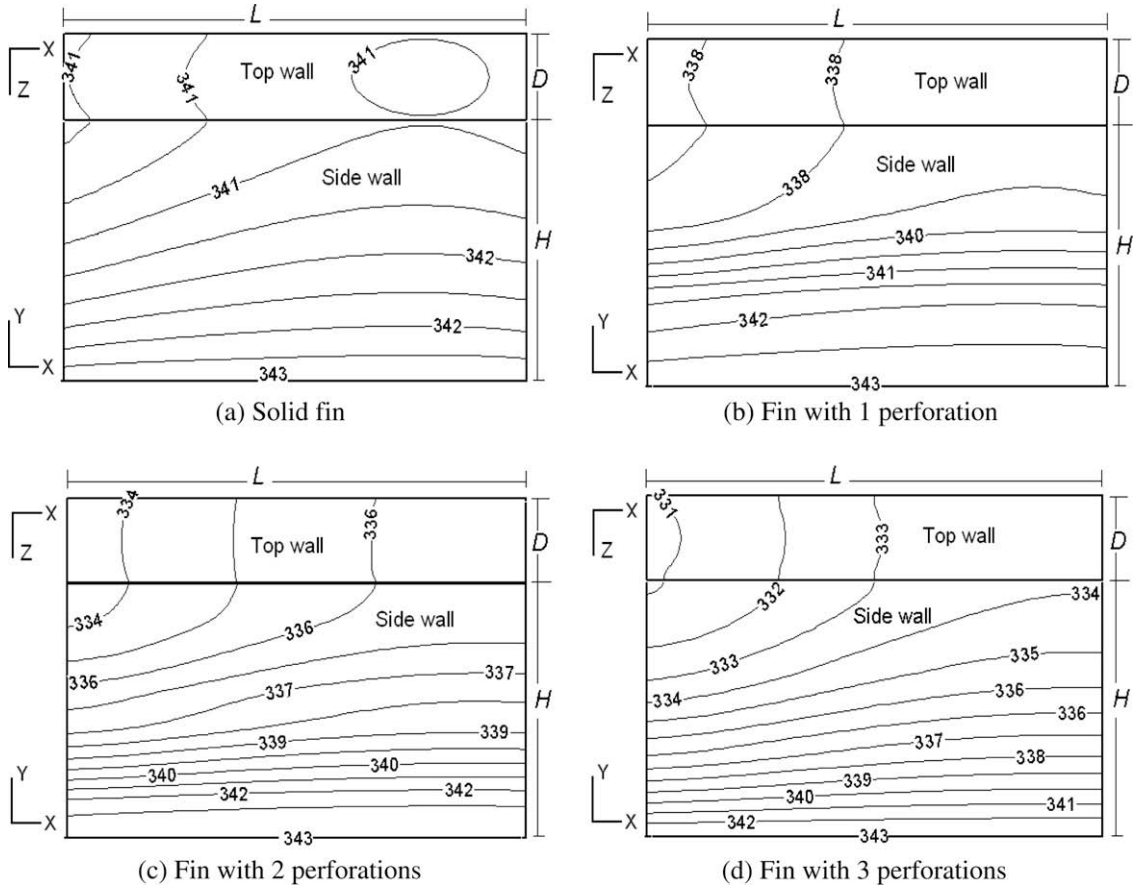

Fig. 11. Isothermal lines over lateral and top surfaces of solid and perforated fins($Re_L = 2.5 \times 10^4$).

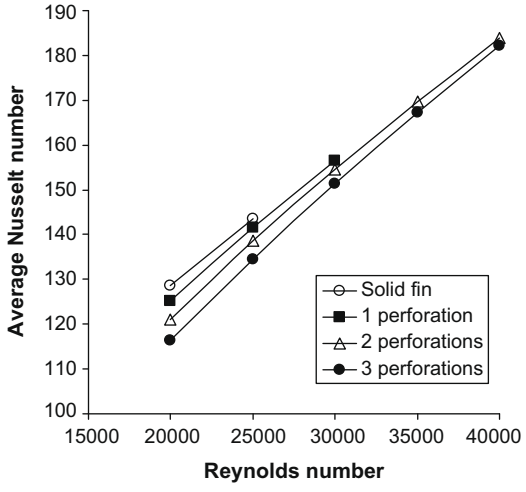

Fig. 12. Variation of average overall Nusselt number over faces of fins.

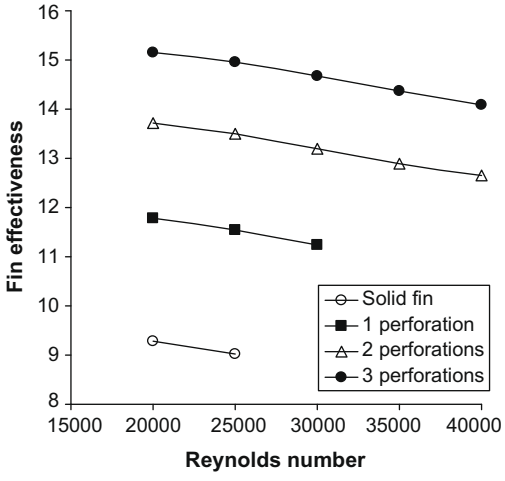

Fig. 13. Variation of fin effectiveness for solid and perforated fins.

of weight in the equipments. With such consideration optimized condition will be achieved.

For practical application of the new perforated fin design, a correlation to predict ε_f with respect to Re_L and porosity $\left(\phi = \frac{V_{void}}{V}\right)$ is proposed. All the numerical values are used and a correlation for fin effectiveness is obtained as:

$$\varepsilon_f = 22.5\ Re_L^{-0.07838}(1-\phi)^{-0.4813} \quad \text{for the range of } Re_L \text{ in Table 1} \tag{17}$$

with accuracy of $R^2 = 0.9$.

Table 3
Percentage increase of heat transfer area of perforated fins in comparison with solid fin.

Fin type	Percentage of increase
Fin with 1 perforation	35.16
Fin with 2 perforations	70.31
Fin with 3 perforations	105.47

Table 4
Percentage weight reduction of perforated fins with comparison of solid fins.

Number of perforations	Percentage of weight reduction
1	18.75
2	37.5
3	56.25

6. Conclusions

In this analysis three-dimensional numerical study of turbulent fluid flow and convective heat transfer over an array of solid and perforated fins are performed. Perforations such as small channels in several numbers are arranged along the length of fins. Effects of flow and perforations on heat transfer rate are determined and comparison between solid and perforated fins is accomplished. Calculations are made for the range of Reynolds numbers from 2×10^4 to 4×10^4 and the following conclusions are made:

(a) At higher Reynolds number the flow around solid fin and perforated fin with 1 perforation is unsteady while by increasing number of perforation, the flow remains steady at the same Reynolds numbers.
(b) Perforated fins have higher contact area with fluid in comparison with solid fin. So the average friction drag for perforated fins is higher compared to solid fin and also it increases by adding perforations.
(c) By increasing number of perforations, the size of formed wake behind the fin decreased. Accordingly the form drag for solid fin is the highest and it decreases with increase of perforations.
(d) Total drag is highest for solid fin and it decreases by increasing perforations. The same result is obtained for average drag coefficient.
(e) By increasing number of perforations, the length of recirculation zone around the lateral surfaces of fin reduced. In fact solid fin has the largest recirculation zone at its lateral surfaces.
(f) Temperature drop from fin base to fin top surface increases with addition of perforations.
(g) Perforated fins have higher fin effectiveness than solid fin and it rises remarkably by adding more perforations. Such increase of fin effectiveness shows the enhancement of heat transfer from perforated fin with respect to solid fin in the range of the present investigation. It should be noted that further increase of perforations will change the rate of heat transfer and an optimum number of perforations may be find for any specific channel size. This needs further investigations and comparison with solid fin. For practical application to predict heat transfer enhancement from individual solid and perforated fins the following correlation is recommended: $\varepsilon_f = 22.5\ Re_L^{-0.07838}(1-\phi)^{-0.4813}$
(h) By increase of perforations, weight reduction is considerable and this economical gain is along with more enhancement of heat transfer rate. Hence by the new fin design both goals of fin optimization for practical applications can achieved.

References

Asako, Y., Faghri, M., 1994. Parametric study of turbulent three-dimensional heat transfer of arrays of heated blocks encountered in electronic equipment. Int. J. Heat Mass Transfer 37 (3), 469–478.
Dorignac, E., Vullierme, J.J., Broussely, M., Foulon, C., Mokkadem, M., 2005. Experimental heat transfer on the windward surface of a perforated flat plate. Int. J. Therm. Sci. 44, 885–893.
El-Sayed, S.A., Mohamed, Sh.M., Abdel-latif, A.A., Abouda, A.-h.E., 2004. Experimental study of heat transfer and fluid flow in longitudinal rectangular-fin array located in different orientations in fluid flow. Exp. Therm. Fluid Sci. 29, 113–128.
Fujii, M., Seshimo, Y., Yamanaka, G., 1988. Heat transfer and pressure drop of perforated surface heat exchanger with passage enlargement and contraction. Int. J. Heat Mass Transfer 31 (1), 135–142.
Hwang, J.J., Liou, T.M., 1995. Heat transfer and friction in a low-aspect-ratio rectangular channel with staggered perforated ribs on two opposite walls. ASME J. Heat Transfer 117, 843–850.
Hwang, J.J., Lia, T.Y., Liou, T.M., 1998. Effect of fences thickness on pressure drop and heat transfer in a perforated-fenced channel. Int. J. Heat Mass Transfer 41, 811–816.
Incropera, F.P., DeWitt, D.P., 1996. Introduction to Heat Transfer. third ed.. John Wiley & Sons, Inc..
Jonsson, H., Moshfegh, B., 2001. Modeling of the thermal and hydraulic performance of plate fin, strip fin, and pin fin heat sinks—influence of flow by pass. IEEE Transactions on Components and Packaging Technologies 24 (2), 142–149.
Leung, C.W., Probert, SD., 1989. Heat exchanger performance: effect of orientation. Appl. Energy 33, 35–52.
Li, H.-Y., Chen, K.-Y., 2007. Thermal performance of plate-fin heat sinks under confined impinging jet conditions. Int. J. Heat Mass Transfer 50, 1963–1970.
Liou, T.M., Chen, S.H., 1998. Turbulent heat and fluid flow in a passage distributed by detached perforated ribs of different heights. Int. J. Heat Mass Transfer 41, 1795–1806.
Meinders, E.R., Van der meer, T.H., Hanjalic, K., 1998. Local convection heat transfer from an array of wall-mounted cubes. Int. J. Heat Mass Transfer 41 (2), 335–346.
Molki, M., Hashemi-Esfahanian, A., 1992. Turbulent convective mass transfer downstream of a perforated baffle blockage. Int. J. Heat Fluid Flow 13 (2), 116–123.
Nakamura, H., Igarashi, T., Tsutsui, T., 2001. Local heat transfer around a wall-mounted cube in the turbulent boundary layer. Int. J. Heat Mass Transfer 44, 3385–3395.
Niceno, B., Dronkers, A.D.T., Hanjalic, K., 2002. Turbulent heat transfer from a multi-layered wall-mounted cube matrix: a large eddy simulation. Int. J. Heat Fluid Flow 23, 173–185.
Nilles, M.J., Calkins, M.E., Dingus, M.L., Hendricks, J.B., 1995. Heat transfer and flow friction in perforated plate heat exchangers. Exp. Therm. Fluid Sci. 10, 238–247.
Patankar, S.V., 1980. Numerical Heat Transfer and Fluid Flow. Hemisphere, Washington, DC.
Razelos, P., Kakatsios, X., 2000. Optimum dimensions of convecting-radiating fins: part I-longitudinal fins. Appl. Therm. Eng. 20, 1161–1192.
Sahin, B., Demir, A., 2008. Performance analysis of a heat exchanger having perforated square fins. Appl. Therm. Eng. 28, 621–632.
Sara, O.N., Pekdemir, T., Yapici, S., Ersahan, H., 2000. Thermal performance analysis for solid and perforated blocks attached on a flat surface in duct flow. Energy Convers. Manage. 41, 1019–1028.
Souidi, N., Bontemps, A., 2001. Countercurrent gas–liquid flow in plate-fin heat exchangers with plain and perforated fins. Int. J. Heat Fluid Flow 22, 450–459.
Sparrow, E.M., Carranco Ortiz, M., 1982. Heat transfer coefficients for the upstream face of a perforated plate positioned normal to an oncoming flow. Int. J. Heat Mass Transfer 25 (1), 127–135.
Torii, S., Yang, W.-J., 2002. Thermal transport phenomena over a slot-perforated flat surface in pulsating free stream. Int. J. Therm. Sci. 41, 241–252.
Velayati, E., Yaghoubi, M., 2005. Numerical study of convective heat transfer from an array of parallel bluff plates. Int. J. Heat Fluid Flow 26, 80–91.
Yaghoubi, M., Amnieh, H., Velayati, E., 2002. Laminar fluid flow and heat transfer from stacks of blunt fins swith finite length. In: Proceedings of ESDA2002, Sixth Biennial Conference on Engineering System Design and Analysis, ESDA2002/ATF-014, Istanbul, Turkey, July 8–11.
Yakut, K., Alemdaroglu, N., Kotcioglu, I., Celik, C., 2006. Experimental investigation of thermal resistance of a heat sink with hexagonal fins. Appl. Therm. Eng. 26, 2262–2271.
Yu, X., Feng, J., Feng, Q., Wang, Q., 2005. Development of a plate-pin fin heat sink and its performance comparisons with a plate fin heat sink. Appl. Therm. Eng. 25, 173–182.